Ag co-catalyst prepared by ultrasonic reduction method for efficient photocatalytic conversion of CO_2 with H_2O using $ZnTa_2O_6$ photocatalyst

Kio KAWATA[†,‡], Shoji IGUCHI[†,*], Shimpei NANIWA[†], Tsunehiro TANAKA[†,#], Masamu NISHIMOTO[‡], Kentaro TERAMURA[†,#,*]

[†] Department of Molecular Engineering, Graduate School of Engineering, Kyoto University, Kyoto-daigaku Katsura, Nishikyo-ku, Kyoto 615−8510, Japan

[‡] Ichikawa Research Center, Sumitomo Metal Mining Co., Ltd., 3-18-5, Nakakokubun, Ichikawa,Chiba 272-8588, Japan

[#] Fukui Institute for Fundamental Chemistry, Kyoto University, Takano Nishibiraki-cho 34-4, Sakyo-ku, Kyoto 606-8103, Japan

Corresponding Authors

Shoji IGUCHI: iguchi.shoji.4k@kyoto-u.ac.jp

Kentaro TERAMURA: teramura.kentaro.7r@kyoto-u.ac.jp

Keywords: CO_2 photoreduction, Ag co-catalyst, Ultrasonic reduction method

Abstract

Toward the realization of carbon neutrality by utilizing renewable energy sources, photocatalytic conversion of CO_2 with H_2O, known as artificial photosynthesis, should be important because H_2O is harmless and an abundant source of protons for CO_2 reduction. Many researchers focusing on the photocatalytic conversion of CO_2 have revealed that the Ag nanoparticle was an effective co-catalyst for the selective conversion of CO_2 to CO in water. To improve the activity for the photocatalytic conversion of CO_2 in water, it is important to modify the surface of the photocatalysts to load small Ag nanoparticles with high dispersity, which is difficult when using conventional methods. In this study, the ultrasonic reduction (USR) method was used as an advanced modification method of photocatalysts with the Ag co-catalyst. We found that $Ag/ZnTa_2O_6$ prepared by the USR method showed good selectivity toward CO (> 90 %) evolution and a higher formation rate of CO than those by conventional modification methods. High-Resolution Transmission Electron Microscopy (HR-TEM) images of the Ag co-catalyst clarified that Ag nanoparticles with the size of a single nanometer were loaded on the surface of $ZnTa_2O_6$ by the USR method, whereas much bigger Ag particles were observed in the case of the other methods. Accordingly, it can be noted that a small Ag co-catalyst with a single nanometer exhibits superior activity toward selective

conversion of CO_2 to CO. We herein successfully achieved a high formation rate of CO with high selectivity using the $Ag/ZnTa_2O_6$ photocatalyst prepared by the USR method.

Introduction

Global warming is causing a rise in sea levels and abnormal weather, beginning to have a negative impact on people's lives and ecosystems. The largest contributor to global warming among greenhouse gases is carbon dioxide (CO_2). To reduce CO_2 emissions, it is important to develop advanced technology for the capture and usage of CO_2, known as CCUS (Carbon Dioxide Capture, Utilization and Storage) rather than decreasing the use of fossil fuels.[1] Among CCUS technologies, artificial photosynthesis based on photocatalysis has been attracting significant attention.[2–5] Particularly, the photocatalytic conversion of CO_2 with H_2O is expected to be applied in practical uses because it enables us to directly reduce CO_2 and produce useful intermediate chemicals for industrial applications, such as CO, CHOOH, HCHO, CH_3OH and CH_4.[6–9] Furthermore, using H_2O as an electron donor is also important to realize artificial photosynthesis like plants because water is harmless and an abundant reductant.

The photocatalytic reduction of CO_2 by H_2O is described by the following equations. When the semiconductor photocatalyst is irradiated with ultraviolet light, which has greater energy than the band gap energy of the photocatalyst, excited electrons (e^-) and holes (h^+) are generated at the conduction band and the valence band of the

photocatalyst, respectively. Then, CO_2 reacts with e^- to produce CO (Eq. 1), while H_2O is oxidized to O_2 (Eq. 2).

$$CO_2 + 2H^+ + 2e^- \rightarrow CO + H_2O \quad \text{(Eq. 1)}$$

$$2H_2O + 4h^+ \rightarrow O_2 + 4H^+ \quad \text{(Eq. 2)}$$

$$2H^+ + 2e^- \rightarrow H_2 \quad \text{(Eq. 3)}$$

The standard redox potential of CO_2 ($E°(CO_2/CO) = -0.11$ V versus standard hydrogen electrode (SHE)) is more negative than that of H^+ ($E°(H^+/H_2) = 0.0$ V versus SHE). This makes H_2 evolution, caused by the reduction of protons (H^+), thermodynamically favorable compared to CO formation via CO_2 reduction. Modifying the photocatalyst surface appropriately is necessary to enhance the selectivity of photogenerated electrons towards the less thermodynamically favored CO_2 reduction. One of the methods for the selective conversion of CO_2 is the modification of photocatalysts by loading metal co-catalysts.[10–12] After Kudo *et al.* reported that the $BaLa_4Ti_4O_{15}$ photocatalyst could be effectively used for the photocatalytic conversion of CO_2 in the presence of a Ag co-catalyst,[6] many research groups including our group concurred that the Ag co-catalyst was crucial for the selective conversion of CO_2 in water.[8, 13–24] As a modification method of Ag co-catalyst, for example, impregnation, photodeposition, chemical reduction, and solution plasma methods have found

widespread use.[19–24] Building upon these methods, in this study, we specifically investigated the ultrasonic reduction (USR) method as an advanced method for modifying the Ag co-catalyst.

In 1991, metal nanoparticles (amorphous iron) were successfully synthesized for the first time by ultrasonic irradiation of solutions containing volatile organometallic compounds.[25] These chemical effects of ultrasound were derived from local high temperatures (> 5000 K) and high pressures (> 1000 atmospheres), known as “hot spots”, formed by the collapse of cavitation bubbles generated in the system during acoustic cavitation.[25–29] After the report by Suslick *et al.*, the syntheses of nanostructured metal particles via ultrasonic reduction were reported by a number of research groups.[30–36] Among these research groups, Hayashi and co-workers found that nanosized noble metals, such as Ag, Au, Pt, and Pd, could be directly synthesized from the reaction of metal oxides (Ag_2O, Au_2O_3, PtO_2, PdO) in alcohol by the USR method.[36,37] Additionally, they synthesized several nanocomposites containing Ag nanoparticles, such as Ag/CNT (carbon nano tube),[38] Ag/Rubber,[39] and $Ag/BaTiO_3$[40].

In the application of the USR method to modify co-catalysts, Pt/TiO_2 or $AuPd/TiO_2$ (core-shell bimetallic co-catalysts) were successfully prepared, demonstrating photocatalytic activity for H_2 evolution from an ethanol aqueous solution.[41,42] However,

to our knowledge, there are no examples of evaluating the activities for the photocatalytic conversion of CO_2 with H_2O over Ag-loaded photocatalysts modified by the USR method, except for our previous report.[43] The USR method is a simplified fabrication method for Ag nanoparticles, synthesized only by irradiating an Ag_2O precursor dispersed in an alcohol solution with appropriate ultrasonic frequency. In our previous study, we found that Ag nanoparticles, with the particle size of approximately 20 nm, were homogeneously loaded on the surface of gallium oxide (Ga_2O_3) particles by irradiating Ag_2O precursors and Ga_2O_3 semiconductor photocatalysts dispersed in an alcohol solution with an appropriate ultrasonic frequency. [43]

In this study, the loading of Ag cocatalyst using the USR method was applied to the zinc tantalate ($ZnTa_2O_6$) photocatalyst, and the photocatalytic conversion of CO_2 with H_2O over the $Ag/ZnTa_2O_6$ photocatalyst was investigated. As previously reported in our group, $ZnTa_2O_6$ photocatalyst modified with Ag co-catalyst showed good activity for the photocatalytic conversion of CO_2, [14] and the photocatalytic activity of the $ZnTa_2O_6$ photocatalyst was successfully improved by appropriate surface modification with additional Zn species. [44] On the other hand, the loading method of Ag co-catalyst has not been optimized for the $ZnTa_2O_6$ photocatalyst. It is expected that the USR method will enable us to modify the surface of $ZnTa_2O_6$ to load Ag nanoparticles with high dispersity

and smaller size, which is essential to improve the activity for the photocatalytic conversion of CO_2 with water.

Experimental Section

Synthesis of $ZnTa_2O_6$

Zinc tantalate ($ZnTa_2O_6$) used in this work was synthesized by a typical solid-state reaction (SSR), as described in our previous report. [45] Stoichiometric amounts of ZnO (99.0 %, FUJIFILM Wako Pure Chemical Corporation, Japan) and Ta_2O_5 (99.9 %, Kojundo Chemical Lab. Co., Ltd., Japan) were impregnated with 5 mL of pure water and ground in an aluminum mortar for 10 min. The wet mixtures were then dried at 383 K overnight and transferred to an aluminum crucible for 50 h of calcination at 1273 K under an air atmosphere. X-ray diffraction (XRD) measurements and ultraviolet-visible diffuse reflectance (UV-vis DR) spectroscopy were performed on the prepared $ZnTa_2O_6$, confirming its successful synthesis (Figure S1 and S2, respectively).

Modification of Ag co-catalyst on $ZnTa_2O_6$

Four different methods of modifying Ag co-catalysts were applied: ultrasonic reduction (USR), chemical reduction (CR), impregnation (IMP), and photodeposition

(PD). As a precursor of Ag, silver oxide (Ag_2O; 99.0 %, FUJIFILM Wako Pure Chemical Corporation, Japan) and silver nitrate ($AgNO_3$; 0.1 M aqueous solution, FUJIFILM Wako Pure Chemical Corporation, Japan) were used for USR and the other conventional methods, respectively.

A mixture of $ZnTa_2O_6$, Ag_2O, and ethanol (50 mL; 99.5 %, Kanto Chemical Co., Inc., Japan) was irradiated with ultrasonic waves for 3 hours using an ultrasonic cleaner (Honda Electronics Co., Ltd., WT-100-M, two-frequency switching mode: 28 kHz and 45 kHz). The temperature of the solution was maintained at 313-318 K. After sonication, the resulting solution was filtered and dried in air at 333 K for 1 h to obtain $Ag/ZnTa_2O_6$_USR.

To prepare $Ag/ZnTa_2O_6$ using the CR method ($Ag/ZnTa_2O_6$_CR), the $AgNO_3$ precursor was reduced by an aqueous NaH_2PO_2 solution (0.4 M prepared in house, a special-grade reagent, FUJIFILM Wako Pure Chemical Corporation, Japan) at 353 K for 1.5 h in an aqueous solution. The filtrate was washed with Milli-Q water and dried at room temperature.

$Ag/ZnTa_2O_6$_IMP was prepared by impregnating $ZnTa_2O_6$ with an aqueous solution of $AgNO_3$ at 353 K for 10 min, followed by evaporation at 353 K for 1 h, and

drying at 353 K. The obtained sample was then calcined at 723 K for 2 h under an air atmosphere.

$ZnTa_2O_6$ powder was dispersed in 1.0 L of ultrapure water, and the resulting suspension was thoroughly degassed by flowing Ar gas. A 0.1 M $AgNO_3$ aqueous solution was added to the suspension as a precursor of Ag co-catalyst, and the resulting system was irradiated for 3 h through a cooling jacket fabricated from quartz glass using a 400-W high-pressure Hg lamp. The obtained sample was named '$Ag/ZnTa_2O_6$_PD'. The amount of Ag species loaded on the $ZnTa_2O_6$ photocatalyst was determined by inductively coupled plasma optical emission spectrometry (ICP–OES, iCAP 7400 ICP-OES DUO, Thermo Fischer Scientific Inc.; see Table S1 and S2).

Photocatalytic activity evaluation

The photocatalytic conversion of CO_2 in water was performed inside a quartz inner irradiation-type reaction vessel using a quasi-flow batch system. The synthesized photocatalyst (0.5 g) was dispersed in an aqueous solution of 0.1 M $NaHCO_3$ (a special grade reagent, Wako, Japan).[8] High purity CO_2 gas (99.999%) was continuously bubbled into the solution at a flow rate of 30 mL min^{-1}. After the removal of dissolved air, the suspension was irradiated with a 400-W high-pressure Hg lamp through a quartz filter

equipped with a cooling water system. The CO, H_2, and O_2 products obtained in the outlet gas were analyzed via gas chromatography (Shimadzu GC-8A) using a flame ionization detector and methanizer equipped with a Shincarbon ST column (carrier gas: N_2) for CO and a thermal conductivity detector equipped with a 5 Å molecular sieve column (carrier gas: Ar) for H_2 and O_2. The selectivity towards CO formation in a mixture of CO and H_2 and the balance between the consumed electrons (e^-) and holes (h^+) were calculated via the following formulas:

$$\text{Selectivity towards CO formation (\%)} = 100 \times \boldsymbol{R_{CO}} / (\boldsymbol{R_{CO}} + \boldsymbol{R_{H_2}}) \qquad \text{(Eq. 4)}$$

$$\text{Consumed } e^-/h^+ = 2\times(\boldsymbol{R_{CO}} + \boldsymbol{R_{H_2}}) / (4\times\boldsymbol{R_{O_2}}) \qquad \text{(Eq. 5)}$$

where $\boldsymbol{R}_{\mathrm{CO}}$, $\boldsymbol{R_{H_2}}$, and $\boldsymbol{R_{O_2}}$ represent the formation rates of CO, H_2, and O_2, respectively.

Characterization

X-ray absorption spectroscopy (XAS) was conducted in both transmission and fluorescence modes at the BL14B2 beamline of the SPring-8 synchrotron radiation facility in Hyogo, Japan. The photon energy was calibrated at the inflection point of the Ag K-edge XANES spectra using a reference Ag metal foil (25524 eV). The samples were analyzed by Ultraviolet-visible (UV-vis) diffuse reflectance spectroscopy using a JASCO V-670 spectrometer equipped with an integrating sphere. Transmission Electron

Microscopy (TEM) images were captured using a field-emission transmission electron microscope (JEM-2100F, JEOL Co., Ltd). Ag co-catalysts were also observed at atomic resolution using High-resolution TEM (HRTEM, JEM-2200FS, JEOL Co., Ltd.).

Results and Discussion

Figure 1 shows the formation rates of H_2, O_2, and CO and the selectivity toward CO evolution for the photocatalytic conversion of CO_2 by H_2O over $Ag/ZnTa_2O_6$ prepared via various Ag modification methods. The e^-/h^+ balance calculated in Eq. 5 was close to 1.0, indicating that H_2O functioned as an electron donor and proton source for the photocatalytic conversion of CO_2. The selectivity toward CO of $Ag/ZnTa_2O_6$_USR was above 90%, and there was no obvious difference among the four Ag modification methods (i.e. USR, CR, IMP, and PD methods). However, the formation rate of CO varied vastly among the four Ag modification methods. The formation rate of CO over the $Ag/ZnTa_2O_6$_USR method was the highest (69.6 μmol h^{-1}) among the four methods, which was at most 2.3 times higher than the formation rate of CO compared to the conventional methods. This difference is not due to the amount of loaded Ag co-catalyst because the amount calculated by ICP-OES measurement is almost the same (see Table S1).

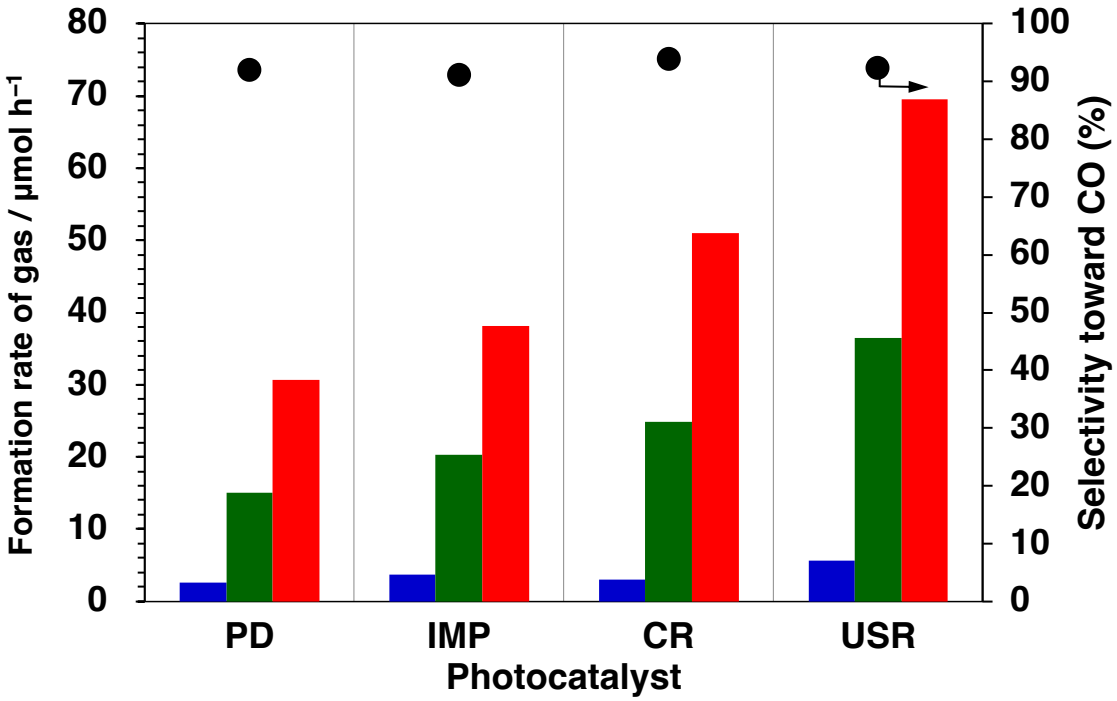

Figure 1 Formation rates of H_2 (blue), O_2 (green), and CO (red), and selectivity toward CO evolution (circle) in the photocatalytic conversion of CO_2 by H_2O over $Ag/ZnTa_2O_6$ with 0.5 wt.% Ag cocatalyst loaded by PD, IMP, CR, and USR.

Figure 2 shows the Ag K-edge X-ray absorption near edge structure (XANES) spectra of Ag/$ZnTa_2O_6$ fabricated using four modification methods. Every Ag K-edge spectrum closely resembles that of Ag foil rather than Ag_2O or $AgNO_3$, which are used as precursors. These results indicate that the Ag precursors were completely reduced to Ag^0, and zero-valent Ag particles were loaded onto the surfaces of $ZnTa_2O_6$ regardless of the method used.

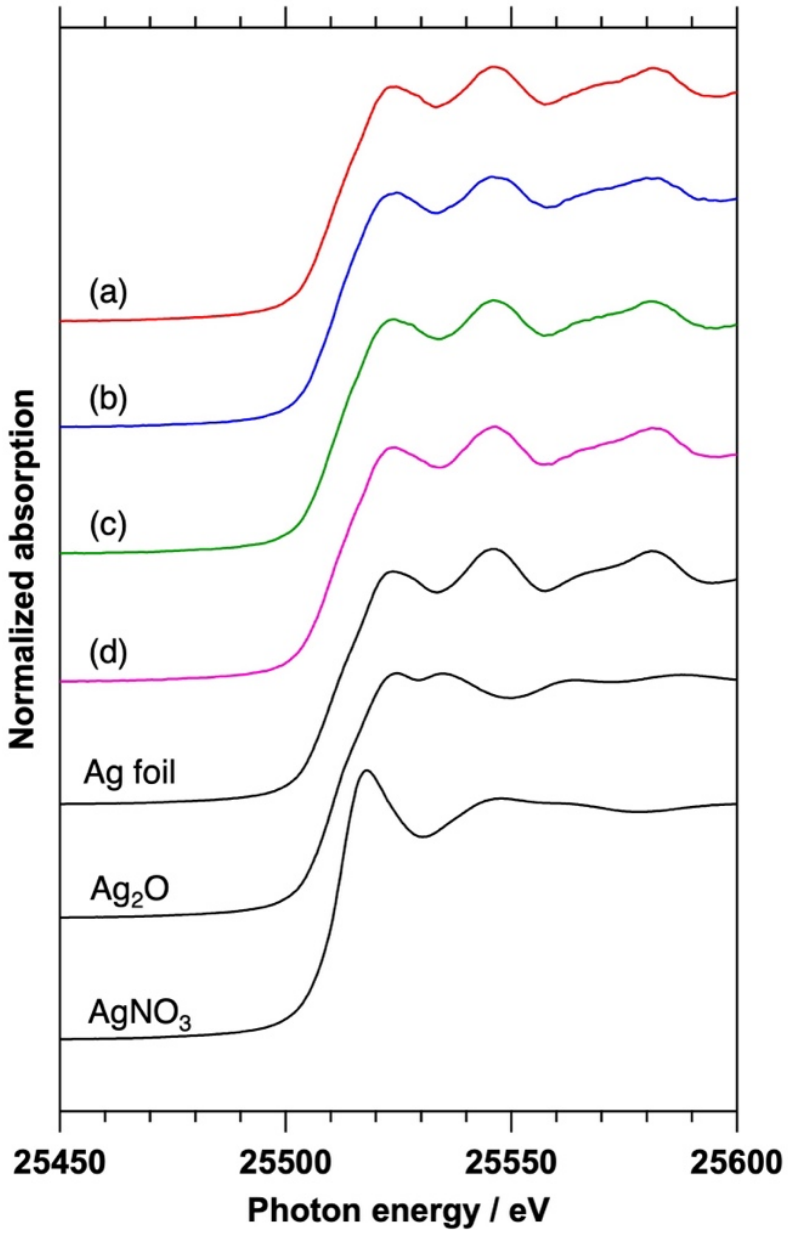

Figure 2 XANES spectra of $ZnTa_2O_6$ with references. Ag species were modified by (a) ultrasonic reduction (USR), (b) chemical reduction (CR), (c) impregnation (IMP), and (d) photodeposition (PD) methods.

The morphology of the Ag co-catalyst on the surface of photocatalysts was observed using TEM (Figure 3 a, c, e, and h). As shown in the TEM images, there were differences in the size and morphology of the Ag nanoparticles on the surface of $ZnTa_2O_6$ among four different kinds of $Ag/ZnTa_2O_6$. The size of Ag nanoparticles on the surface of $ZnTa_2O_6$ prepared by USR, CR, and IMP methods seemed to be almost the same (Figures 3 (a), (c), and (e), respectively), while larger Ag particles were observed on $Ag/ZnTa_2O_6$ fabricated by the PD method (Figure 3 (g)). However, only two Ag nanoparticles were observed on $Ag/ZnTa_2O_6$ prepared by the USR method at the magnification and the field displayed in Figure 3 (a), while more Ag nanoparticles were observed on the surface of $ZnTa_2O_6$ fabricated by CR and IMP methods (Figures 3 (c) and (e), respectively). This result suggests that much smaller-sized Ag nanoparticles are loaded on the surface of $ZnTa_2O_6$ modified by the USR method.

To observe such smaller Ag nanoparticles, TEM observations at the atomic resolution level were conducted. As shown in Figure 3 (b), Ag particles with sizes ranging from 1 to 3 nm exist on the surface of $ZnTa_2O_6$ prepared by the USR method. On the other hand, only Ag nanoparticles over 5 nm were observed on the surface of $ZnTa_2O_6$ loaded by other conventional methods (Figure 3 (d), (f), and (h)). Because there are many CO_2 reduction sites on $Ag/ZnTa_2O_6$ prepared by the USR method compared to other

photocatalysts owing to Ag nanoparticles with a size of a single nanometer, Ag/$ZnTa_2O_6$ modified by the USR method showed high formation rate of CO while maintaining high selectivity toward CO. Therefore, to obtain a high conversion of CO_2 using H_2O as an electron donor, it is important to prepare small Ag nanoparticles on the surface of $ZnTa_2O_6$, and this is achievable by using the USR method as a loading method of Ag co-catalyst.

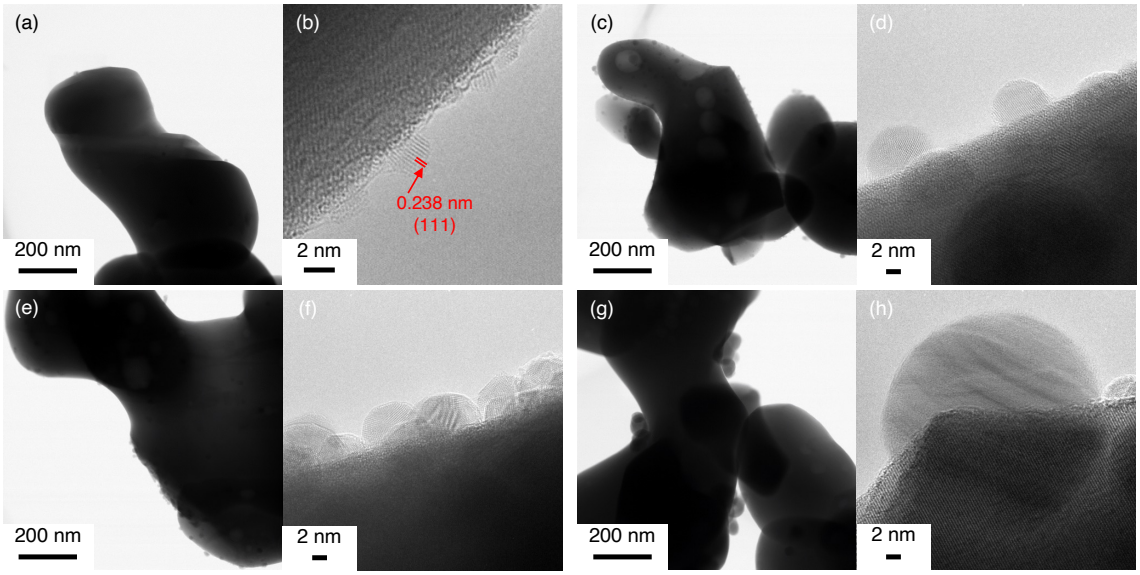

Figure 3 (a, c, e, and g) TEM and (b, d, f, and h) high-resolution TEM (HRTEM) images of $Ag/ZnTa_2O_6$ modified by (a, b) ultrasonic reduction (USR), (c, d) chemical reduction (CR), (e,f) impregnation (IMP), and (g, h) photodeposition (PD) methods.

Ultraviolet–visible (UV-vis) diffuse reflectance spectra of Ag/$ZnTa_2O_6$ fabricated by four different methods are shown in Figure 4. The absorption peak and edge of $ZnTa_2O_6$ at wavelength of 200 to 300 nm were not changed even after Ag was loaded by four modification methods. The absorption peak at wavelengths longer than 300 nm is thought to be due to the surface plasmon resonance of Ag nanoparticles.[20,23,46,47] The peak intensity assigned to plasmon absorption for Ag/$ZnTa_2O_6$ prepared by the USR method was smaller than that by other conventional methods. Plasmonic absorption appears when the Ag particles are in the metallic state and the particle size is in the range of a few nm to hundreds. [20,47] In the case of Ag co-catalyst on $ZnTa_2O_6$ fabricated by the USR method, as well as the conventional ones, Ag was in the metallic state and no particles over 100 nm were observed. Consequently, UV-vis diffuse reflectance spectra suggest that many Ag nanoparticles with a size in the single nanometer range are loaded on $ZnTa_2O_6$ when using the USR method as the fabricating method, supporting the results of TEM observation.

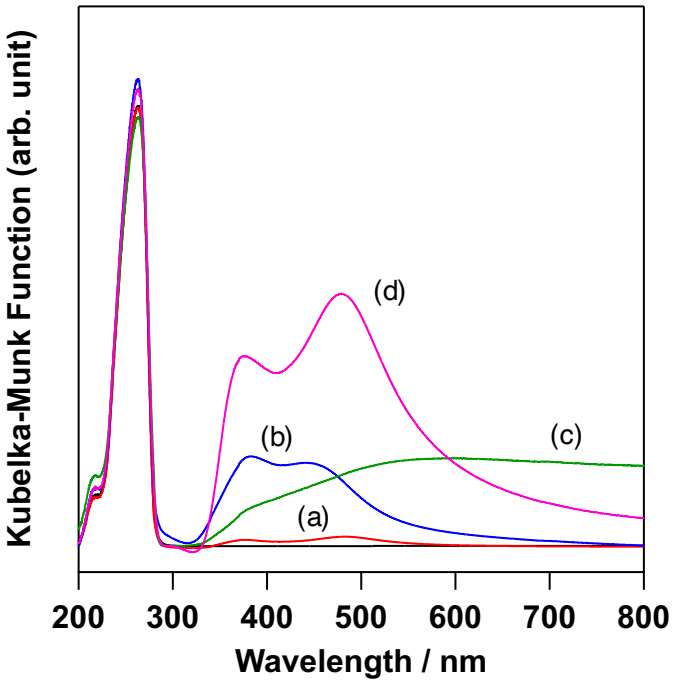

Figure 4 UV-vis diffuse reflectance spectra of $Ag/ZnTa_2O_6$ modified by (a) ultrasonic reduction (USR), (b) chemical reduction (CR), (c) impregnation (IMP), and (d) photodeposition (PD) methods.

As depicted in Figure S3, the formation rate of CO over $Ag/ZnTa_2O_6$ using the USR method decreased more rapidly with an increase in photoirradiation time compared to those employing other modification methods of Ag co-catalysts. This phenomenon can be attributed to the change in the size of Ag nanoparticles on the surface during the reaction. Larger Ag nanoparticles were observed after the photocatalytic reaction using TEM equipment (as illustrated in Figure S4). Furthermore, the intensity of the broad peak in UV-vis DRS, assigned to plasmon absorption by Ag nanoparticles, increased after the photocatalytic reaction (Figure S5). This increase suggests that the smaller Ag particles present before the reaction tend to aggregate into larger particles.[19] Consequently, the rapid decrease in the formation rate of CO over $Ag/ZnTa_2O_6$ by the USR method is attributed to the existence of smaller Ag nanoparticles before the photocatalytic reaction, thus corroborating the results depicted in Figure 4.

Figure 5 illustrates the formation rates of H_2, O_2, and CO, as well as the selectivity toward CO evolution in the photocatalytic conversion of CO_2 by H_2O over $Ag/ZnTa_2O_6$ with various loading amounts of Ag co-catalyst fabricated by the USR method. The formation rate of CO and selectivity toward CO increased from 13 μmol h^{-1} and 46 % to approximately 50 μmol h^{-1} and 80 %, respectively, upon modification with 0.1 wt.% Ag co-catalyst. Furthermore, as the loading amount of Ag was increased to 0.5

wt.%, the formation rate of CO evolved also increased, accompanied by a decrease in H_2 evolution. This improvement is attributed to the increase in the number of CO_2 reduction sites. The amount of Ag co-catalyst loaded on $ZnTa_2O_6$, where the formation rate of CO was maximum, was 0.5 wt.% when using the USR method as a modification method of Ag co-catalyst. On the other hand, the optimized amount was 3.0 wt.% when using the conventional modification method. [14,44,45] By using the USR method, not only can the photocatalytic activity be higher, but also the optimized amount of Ag co-catalyst can be smaller. This is because Ag co-catalyst with a single nanometer can be loaded on $ZnTa_2O_6$ by the USR method.

The modification with higher amounts of Ag (above 1.0 wt.%) led to a gradual decrease in the activity for photocatalytic CO_2 reduction. This decrease might be because Ag nanoparticles play the role of recombination centers for electrons and holes, and they also have a shielding effect on ultraviolet light.[48.49] Certainly, as shown in Figure S6, absorption at around 300 nm appeared when the loading amount of Ag co-catalyst was 2.0 wt.% or higher, which overlaps with the absorption by $ZnTa_2O_6$, causing the decrease in photocatalytic activity. The formation rate of CO, however, decreases more rapidly in the range of 0.5 to 2.0 wt.% of Ag co-catalyst rather than in the range of 2.0 to 5.0 wt.%, even though $Ag/ZnTa_2O_6$ with 2.0–5.0 wt.% Ag co-catalyst exhibits more factors

contributing to the lowering of photocatalytic activity. Consequently, another factor should be considered.

At 1.0 wt.% or a higher amount of Ag co-catalyst, more Ag particles can be observed by TEM at the magnification displayed in Figure S7. Furthermore, UV-vis diffuse reflectance spectra shown in Figure S6 indicate that the peak intensity assigned to plasmon absorption of Ag nanoparticles increased as the amount of Ag co-catalysts increased, suggesting that the population of Ag nanoparticles increased. Based on these characterizations, we consider that the decrease in photocatalytic activity is due to the existence of more Ag particles with a larger size, rather than a singular nanometer, as the loading amount of Ag co-catalyst increases. In fact, as shown in Figure 6, a clear correlation was observed between the formation rate of CO and the average size of Ag particles, suggesting that smaller Ag nanoparticles are more effective for the photocatalytic conversion of CO_2. Although several previous studies demonstrated that the volcano plot was observed in the relationship between the formation rate of CO and the average size of Ag particles,[50–52] the linear relationship between them suggests that the perimeter of Ag particles may be a key factor for the photocatalytic conversion of CO_2.[53] In other words, a peak top of the volcano plot in the case of the USR method should be found at a much smaller size region.

Two mechanisms of Ag nanoparticle formation from Ag_2O via the ultrasonic reduction method are proposed. [37,54,55] The first one is the direct decomposition and reduction of Ag_2O in hot spots by ultrasonic cavitation. In this process, hot spots act directly on the surface of silver oxide particles, and Ag_2O on the surface is thermally decomposed and reduced to Ag nanoparticles. When Ag nanoparticles grow to about 50 nm on the surface, the interfacial stress between Ag_2O and Ag nanoparticles reaches a limit, and the Ag nanoparticles are desorbed. The second mechanism is a reaction through intermediate products, such as silver acetate. Ethanol reacts with Ag_2O by ultrasonic waves to form silver acetate. The silver acetate is decomposed in the hot spot to form Ag nanoparticles. It is considered that the silver acetate is formed and decomposed sequentially in small quantities, resulting in the formation of smaller nanoparticles compared to the former reaction mechanism.[54,55]

In the case of our photocatalyst, we consider the latter mechanism to be dominant because few Ag nanoparticles, with a size of about 50 nm or larger, were observed regardless of the loading amount of Ag co-catalyst (refer to the Ag particle size distribution on $Ag/ZnTa_2O_6$ with various loading amounts of Ag co-catalyst shown in Figure S8). Hot spots produced by ultrasonic irradiation were generated randomly in the ethanol solution. Therefore, the heterogeneous nucleation of Ag in the solution occurred,

followed by the growth and immobilization of the Ag particles on the surface of $ZnTa_2O_6$ while uniformly dispersing them. The increase in size with increasing loading amount of Ag co-catalyst was due to the aggregation of small Ag nanoparticles. Consequently, the small Ag nanoparticles are loaded on the surface of $ZnTa_2O_6$ when the Ag co-catalyst has a low loading amount. From our study, we can therefore conclude that it is essential to prepare small Ag nanoparticles on the surface of $ZnTa_2O_6$ to obtain high conversion of CO_2 using H_2O as an electron donor, and this can be achieved by using the ultrasonic reduction method as a loading method of Ag co-catalyst.

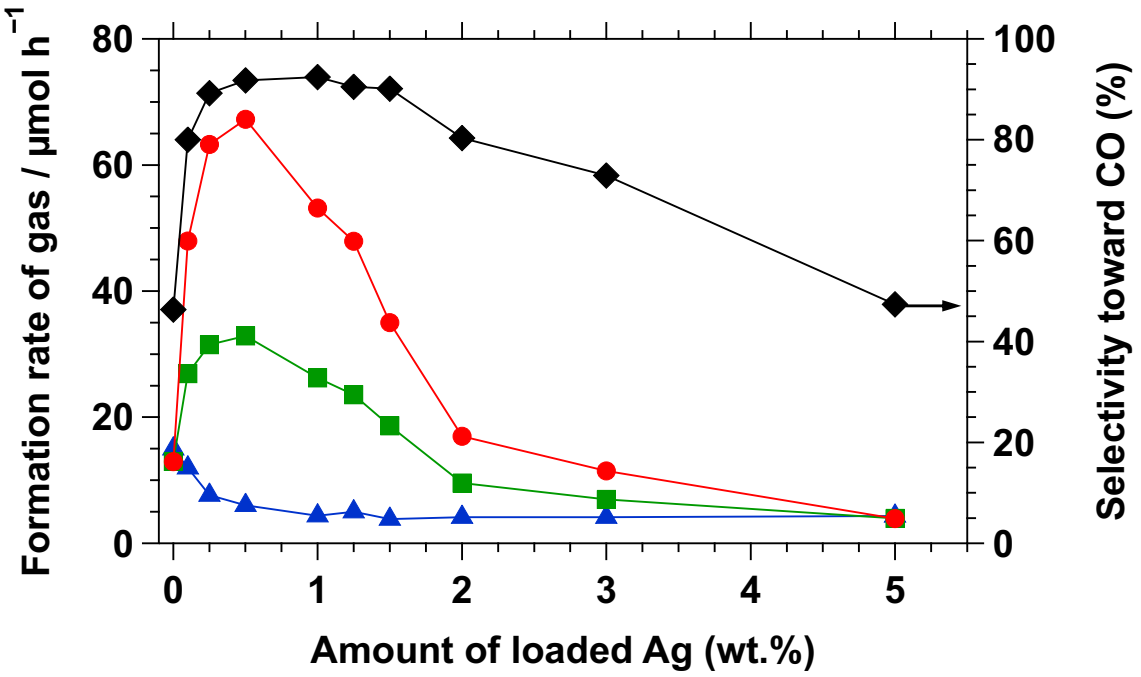

Figure 5 Formation rates of H_2 (blue), O_2 (green), and CO (red), and selectivity toward CO evolution in the photocatalytic conversion of CO_2 by H_2O over $Ag/ZnTa_2O_6$ with various loading amounts of Ag fabricated by the USR method.

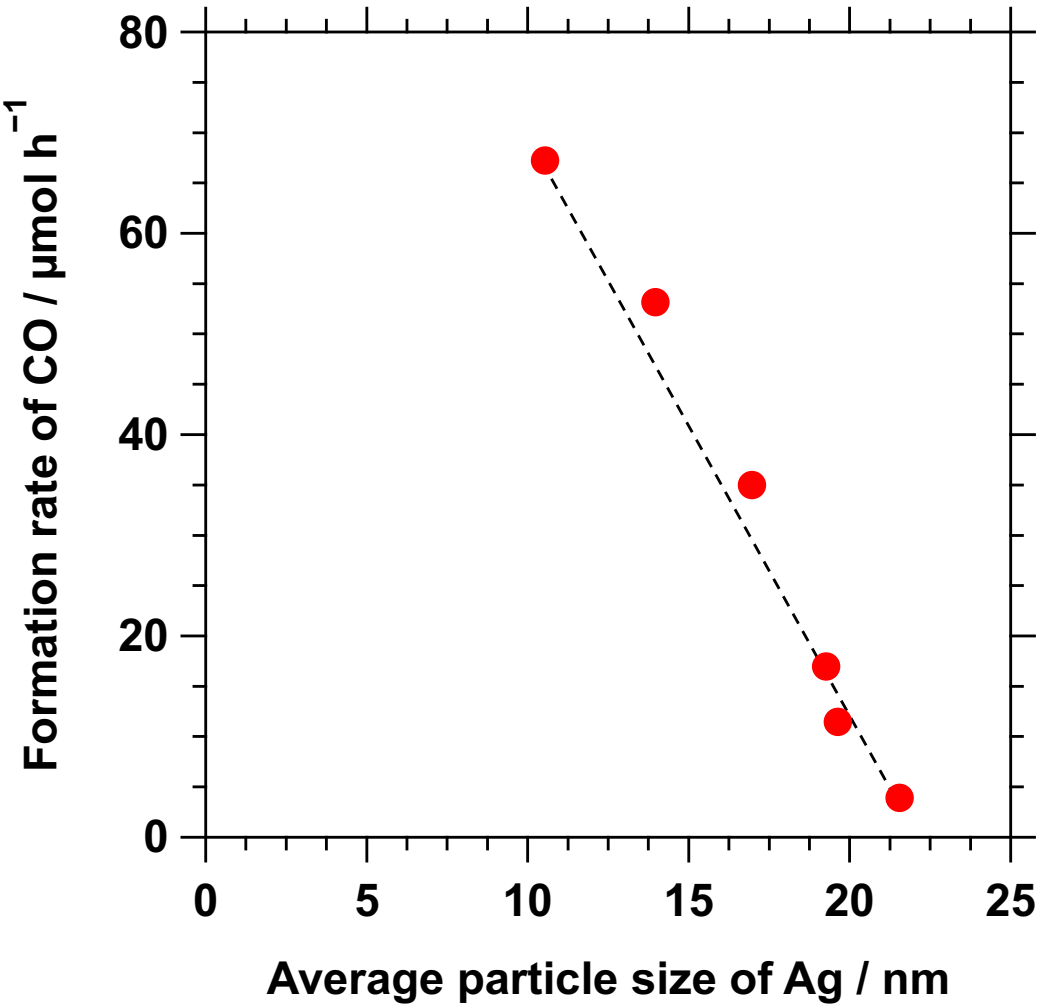

Figure 6 Dependence of the average particle size of Ag on the formation rate of CO.

Conclusions

In this study, we found that the photocatalytic activity of the $ZnTa_2O_6$ photocatalyst for the conversion of CO_2 was significantly improved by modifying it with an Ag co-catalyst using the ultrasonic reduction (USR) method. Ag nanoparticles with sizes ranging from 1 to 3 nm were loaded onto the surface of $ZnTa_2O_6$ prepared by the USR method. Conversely, the average diameter of Ag particles fabricated by other methods was much larger than those produced by the USR method. Therefore, small Ag co-catalysts with single nanometer dimensions exhibited superior activity toward the selective conversion of CO_2. By utilizing the $Ag/ZnTa_2O_6$ photocatalyst prepared via the USR method, a high formation rate of CO with high selectivity toward CO can be achieved.

Supporting Information

The Supporting Information is available free of charge at ***

XRD patterns of (a) $ZnTa_2O_6$ and (b) reference patterns of $ZnTa_2O_6$ (ICSD #36289), Ultraviolet–visible (UV-vis) diffuse reflectance spectrum of $ZnTa_2O_6$, The amount of loaded Ag co-catalyst on $ZnTa_2O_6$ ($Ag/ZnTa_2O_6$) fabricated by the four different modification methods (i.e. USR, CR, IMP, and PD). The total amount of loaded

Ag species was determined by analyzing solution after dissolving $Ag/ZnTa_2O_6$ in concentrated nitric acid via inductively coupled plasma optical emission spectrometry (ICP–OES, iCAP 7400 ICP-OES DUO, Thermo Fischer Scientific Inc.), The amount of loaded Ag co-catalyst on $ZnTa_2O_6$ ($Ag/ZnTa_2O_6$) fabricated by the USR method, Time courses of formation rates of CO over $Ag/ZnTa_2O_6$ catalysts prepared by (a) an ultrasonic reduction (USR), (b) a chemical reduction (CR), (c) an impregnation (IMP), and (d) a photodeposition (PD) methods, TEM images of $Ag/ZnTa_2O_6$ modified by the USR method; (a) before and (b) after photocatalytic reaction, UV-vis diffuse reflectance spectra of $Ag/ZnTa_2O_6$ modified by the USR method (a) before and (b) after photocatalytic reaction, UV-vis diffuse reflectance spectra of $Ag/ZnTa_2O_6$ with various loading amounts of Ag fabricated by the USR method, TEM images of $Ag/ZnTa_2O_6$ with various loading amounts of Ag fabricated by the USR method; (a) 0.1, (b) 0.5, (c) 1.0, (d) 2.0, (e) 3.0, and (f) 5.0 wt.%, The size distribution of Ag particles on the surface of $ZnTa_2O_6$ with various loading amounts of Ag fabricated by the USR method; (a) 0.5, (b) 1.0, (c) 1.5, (d) 2.0, (e) 3.0, and (f) 5.0 wt.%

Acknowledgements

The XAS measurements were performed at the BL14B2 of SPring-8 with the approval of the Japan Synchrotron Radiation Research Institute (JASRI) (Proposal No. 2022B1885). TEM observations at the atomic resolution level were conducted at the Advanced Research Infrastructure for Materials and Nanotechnology in Japan (ARIM Japan). This work was partially supported by "The Mitsubishi Foundation".

References

[1] J. R. Fernández, S. Garcia, E. S. Sanz-Pérez, *Ind. Eng. Chem. Res.*, **2020**, *59*, 6767−6772.

[2] K. Maeda, *J. Photochem. Photobiol. C*, **2011**, *12*, 237–268.

[3] S. Xie, Q. Zhang, G. Liu, Y. Wang, *Chem. Commun.*, **2016**, *52*, 35–59.

[4] S. Chen, Y. Qi, C. Li, K. Domen, F. Zhang, *Joule*, **2018**, *2*, 2260–2288.

[5] Y. Wang, D. He, H. Chen, D. Wang, *J. Photochem. Photobiol. C*, **2019**, *40*, 117–149.

[6] K. Iizuka, T. Wato, Y. Miseki, K. Saito, A. Kudo, *J. Am. Chem. Soc.*, **2011**, *133*, 20863–20868.

[7] M. Yamamoto, T. Yoshida, N. Yamamoto, H. Yoshida, S. Yagi, *e-J. Surf. Sci. Nanotech.*, **2014**, *12*, 299–303.

[8] K. Teramura, T. Tanaka, *Phys. Chem. Chem. Phys.*, **2018**, *20*, 8423–8431.

[9] J. Artz, T. E. Müller, K. Thenert, J. Kleinekorte, R. Meys, A. Sternberg, A. Bardow, W. Leitner, *Chem. Rev.*, **2018**, *118*, 434–504.

[10] A. Kudo, Y. Miseki, *Chem. Soc. Rev.*, **2009**, *38*, 253–278.

[11] R. Daghrir, P. Drogui, D. Robert, *Ind. Eng. Chem. Res.*, **2013**, *52*, 3581–3599.

[12] H. Abdullah, M. M. R. Khan, H. R. Ong, Z. Yaakob, *J. CO_2 Util.*, **2017**, *22*, 15–32.

[13] Z. Wang, K. Teramura, S. Hosokawa, T. Tanaka, *J. Mater. Chem. A*, **2015**, *3*, 11313–11319.

[14] S. Iguchi, K. Teramura, S. Hosokawa, T. Tanaka, *Catal. Sci. Technol.*, **2016**, *6*, 4978–4985.

[15] Z. Huang, S. Yoshizawa, K. Teramura, H. Asakura, S. Hosokawa, T. Tanaka, *ACS Sustainable Chem. Eng.*, **2018**, *6*, 8247–8255.

[16] M. Takemoto, Y. Tokudome, S. Kikkawa, K. Teramura, T. Tanaka, K. Okada, H. Murata, A. Nakahira, M. Takahashi, *RSC Adv.*, **2020**, *10*, 8066–8073.

[17] S. Wang, K. Teramura, T. Hisatomi, K. Domen, H. Asakura, S. Hosokawa, T. Tanaka, *Chem. Sci.*, **2021**, *12*, 4940–4948.

[18] T. Nakamoto, S. Iguchi, S. Naniwa, T. Tanaka, K. Teramura, *Catal. Sci. Technol.*, **2023**, *13*, 4534–4541.

[19] K. Teramura, H. Tatsumi, Z. Wang, S. Hosokawa, T. Tanaka, *Bull. Chem. Soc. Jpn.*, **2015**, *88*, 431–437.

[20] M. Yamamoto, T. Yoshida, N. Yamamoto, T. Nomoto, Y. Yamamoto, S. Yagi, H. Yoshida, *J. Mater. Chem. A*, **2015**, *3*, 16810–16816.

[21] M. Yamamoto, T. Yoshida, N. Yamamoto, T. Nomoto, S. Yagi, *Nucl. Instrum. Methods Phys. Res. B*, **2015**, *359*, 64–68.

[22] R. Pang, K. Teramura, H. Asakura, S. Hosokawa, T. Tanaka, *Appl. Catal. B*, **2017**, *218*, 770–778.

[23] T. Yoshida, N. Yamamoto, T. Mizutani, M. Yamamoto, S. Ogawa, S. Yagi, H. Nameki, H. Yoshida, *Catal. Today*, **2018**, *303*, 320–326.

[24] Y. Kawaguchi, M. Akatsuka, M. Yamamoto, K. Yoshioka, A. Ozawa, Y. Kato, T. Yoshida, *J. Photochem. Photobiol. A*, **2018**, *358*, 459–464.

[25] K. S. Suslik, S. Choe, A. A. Cichowlas, M. W. Grinstaff, *Nature*, **1991**, *353*, 414–416.

[26] J. P. Loriner, T. J. Mason, *Chem. Soc. Rev.*, **1987**, *16*, 239–274.

[27] K. S. Suslick, *Science*, **1990,** *247***,** 1439–1445.

[28] K. S. Suslick, G. J. Price, *Annu. Rev. Mater. Sci.*, **1999**, *29*, 295–326.

[29] C. Kan, W. Cai, C. Li, L. Zhang, H Hofmeister, *J. Phys. D: Appl. Phys.*, **2003**, *36*, 1609–1614.

[30] J. Zhang, J. Du, B. Han, Z. Liu, T. Jiang, Z. Zhang, *Angew. Chem. Int. Ed.*, **2006**, *45*, 1116–1119.

[31] N. A. Dhas, C. P. Raj, A. Gedanken, *Chem. Mater*. **1998**, *10*, 1446–1452.

[32] Y. Mizukoshi, R. Oshima, Y. Maeda, Y. Nagata, *Langmuir*, **1999**, *15*, 2733–2737.

[33] R. A. Caruso, M. Ashokkumar, F. Grieser, *Langmuir*, **2002**, *18*, 7831–7836.

[34] C. H. Su, P. L. Wu, C. S. Yeh, *J. Phys. Chem. B*, **2003**, *107*, 14240–14243.

[35] A. Nemamcha, J. L. Rehspringer, D. Khatmi, *J. Phys. Chem. B*, **2006**, *110*, 383–387.

[36] Y. Hayashi, T. Sekino, K. Niihara, *Trans. Mat. Res. Soc. Jpn.*, **2002**, *27*, 121–124.

[37] Y. Hayashi, H. Takizawa, M. Inoue, K. Niihara, K. Suganuma, *IEEE Trans. Electron. Packag. Manuf.*, **2005**, *28*, 383–343.

[38] T. Yamada, Y. Hayashi, H. Takizawa, *Materials Transactions*, **2010**, *51*, 1769–1772.

[39] Y. Hayashi, D. Ishikawa. H. Takizawa, M. Inoue, K. Suganuma, K.Niihara, *J. Jpn. Soc. Powder Powder Metallurgy*, **2007**, *54*, 186–193.

[40] Y. Hayashi, T. Shishido, K. Seki, H. Takizawa, *J. Asian Ceram. Soc.*, **2023**, *11*, 464–471.

[41] Y. Mizukoshi, Y. Makise, T. Shuto, J. Hu, A. Tominaga, S. Shironita, S. Tanabe, *Ultrason. Sonochem.*, **2007**, *14*, 387–392.

[42] Y. Mizukoshi, K. Sato, T. J. Konno, N. Masahashi, *Appl. Catal. B-Environ.*, **2010**, *94*, 248–253.

[43] M. Nishimoto, Y. Abe, K. Teramura, T. Tanaka, *J. Jpn. Soc. Powder Powder Metallurgy*, **2021**, *68*, 93–98.

[44] S. Wang, K. Teramura, H. Asakura, S. Hosokawa, T. Tanaka, *J. Phys. Chem. C*, **2021**, *125*, 1304−1312.

[45] X. Xu, H. Asakura, S. Hosokawa, T. Tanaka, K. Teramura, *Appl. Catal. B-Environ.*, **2023**, *320*, 121885.

[46] X. Zhu, A. Anzai, A. Yamamoto, H. Yoshida, *Appl. Catal. B-Environ.*, **2019**, *243*, 47–56.

[47] J. Zhang, S. Xu, E. Kumacheva, *Adv. Mater.*, **2005**, *17*, 2336–2340.

[48] K. C. Christoforidis, P. Fornasiero, *ChemCatChem.*, **2017**, *9*, 1523–1544.

[49] A. Primo, T. Marino, A. Corma, R. Molinari, H. García, *J. Am. Chem. Soc.*, **2011**, *133*, 6930–6933.

[50] R. Kaur, B. Pal, *J. Mol. Catal. A: Chemical*, **2012**, *355*, 39–43.

[51] F. F. Schweinberger, M. J. Berr, M. Döblinger, C. Wolff, K. E. Sanwald, A. S.Crampton, C. J. Ridge, F. Jaĉkel, J. Feldmann, M.Tschurl, U. Heiz, *J. Am. Chem. Soc.*, **2013**, *135*, 13262–13265.

[52] M. Eder, C. Courtois, P. Petzoldt, S. Mackewicz, M. Tschurl, U. Heiz, *ACS Catal.*, **2022**, *12*, 9579–9588.

[53] M. Yamamoto, A. Kuwabara, T. Yoshida, *ACS Omega*, **2021**, *6*, 33701–33707.

[54] K. Toisawa, Y. Hayashi, H. Takizawa, *Materials Transactions*, **2010**, *51*, 1764–1768.

[55] Y. Hayashi, H. Takizawa, *J. Jpn. Soc. Powder Powder Metallurgy*, **2016**, *63*, 929–936.